# SACLANT ASW RESEARCH CENTRE REPORT



# A FAST FIELD MODEL FOR THREE-DIMENSIONAL WAVE PROPAGATION IN STRATIFIED ENVIRONMENTS BASED ON THE GLOBAL MATRIX METHOD

by

Henrik SCHMIDT
John GLATTETRE

MARCH 1986

NORTH ATLANTIC TREATY ORGANIZATION

SACLANT ASW Research Centre
Viale San Bartolomeo 400,
I-19026 San Bartolomeo (SP), Italy.

tel: $\dfrac{\text{national} \qquad 0187\ 540111}{\text{international} + 39\ 187\ 540111}$

telex: 271148 SACENT I

A FAST FIELD MODEL FOR THREE-DIMENSIONAL
WAVE PROPAGATION IN STRATIFIED ENVIRONMENTS
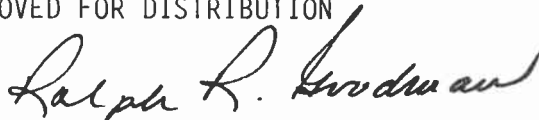BASED ON THE GLOBAL MATRIX METHOD

by

Henrik  Schmidt
John Glattetre

March 1986

This report has been prepared as part of Project 19.

APPROVED FOR DISTRIBUTION

RALPH R. GOODMAN
Director

# A fast field model for three-dimensional wave propagation in stratified environments based on the global matrix method

H. Schmidt
*SACLANT ASW Research Centre, I-10926 La Spezia, Italy*

J. Glattetre[a]
*Norwegian Defence Research Establishment, Division for Underwater Defence, P.O. Box 115, N-3191 Horten, Norway*

A three-dimensional fast field program (FFP) model based on the global matrix method will be presented. Compared to traditional propagator matrix methods, the global matrix method allows for a more efficient, and, furthermore, numerically stable computation. The three-dimensional expansion does not restrict sources to be on the center axis, but allows for an arbitrary source geometry—as opposed to earlier two-dimensional versions. As a consequence, the solution includes simultaneously both vertically and horizontally polarized shear waves. A mathematical description will be given and the numerical aspects will be discussed. Some of the features of the model will be illustrated in two test cases: free-space and shallow water with strongly reflecting bottom. The free-space case shows that the three-dimensional solution gives results identical to those obtained by the two-dimensional model except for ranges close to the axis $r=0$ of a cylindrical coordinate system. For the shallow water case, the well-known energy transportation in discrete modes above critical wavenumber is first demonstrated. Then the model is used to analyze the field radiated by a long horizontal array, and it is shown that different modes will propagate in slightly different directions.

PACS numbers: 43.30.Bp, 43.30.Es, 43.20.Bi

## INTRODUCTION

It is well known that the use of integral transform techniques yields an exact solution to the wave equation in stratified elastic media.[1] The field parameters are, however, determined by inverse transform integrals. In cases with only a few layers, contour integration can be used to reduce the numerical computation, involving only a few integrations over finite intervals (e.g., see Ref. 1). In general numerical models, however, such techniques are inconvenient, and direct numerical integration has to be used.

In underwater acoustics the sources are usually contained within a small volume, in comparison to the volume of interest; thus the radiated field is most conveniently described in a cylindrical coordinate system. In this case the field is given by Hankel transform integrals which are not well suited for direct numerical integration due to the Bessel functions involved. In order to overcome this problem, in 1961 Marsh[2] introduced what was later called the fast field approximation of the Hankel transform. The field is separated into ingoing and outgoing parts by expressing the Bessel function in terms of Hankel functions which are then replaced by their large argument approximations. The integrals are then evaluated by means of the fast Fourier transform. As shown later by Di Napoli and Deavenport,[3] the fast field approximation gives no significant errors at ranges longer than a few wavelengths from the axis.

After the introduction of the fast field technique, a number of numerical models have been developed based on this integration method, and thus are usually called fast field programs. In spite of their common name, these models are significantly different, especially concerning the approach taken to solve the transformed wave equations in a multilayered environment. Traditionally, the depth dependence of the field has been determined by means of the Thomson–Haskell matrix method.[4,5] The first model was introduced by DiNapoli,[6] who evaluated the solution very efficiently by means of recurrence relations for the hypergeometric functions. However, this approach allows only for fluid layers, and in that case, other techniques, like normal mode methods, are usually more convenient. The first FFP model, including the coupling between $P$ and $SV$ waves at the boundaries of solid layers, was developed by Kutschale[7] also using the Thomson–Haskell method. The original model allowed for only one source/receiver combination for each solution. It was later modified by Harrison[8] to allow for several receivers, but even for one combination the computations are rather extensive.

A more direct and computationally more efficient solution technique was recently introduced by Schmidt.[9] The field parameters at the interfaces are expressed in terms of source contributions and unknown scalar potentials. The boundary conditions yield a system of equations in the Hankel transforms of the potentials to be satisfied at each interface. These local systems of equations are mapped into a global set of equations using a technique similar to the one used in finite element programs. The computational speed

has been improved by an order of magnitude by use of this solution technique. Furthermore, configurations involving several sources and/or receivers can be treated with one solution, thus yielding the possibility of computing total fields generated not only by single point sources, but also by vertical source arrays.

These and similar models have all been two dimensional, thus restricting the sources to be placed on the axis of the cylindrical coordinate system. A direct solution of problems with horizontally distributed sources has, therefore, not been possible, but has required a new calculation for each source and subsequent superposition. In this paper the model of Schmidt[9] has been modified and extended to allow for sources displaced with respect to the axis.

The field parameters are expanded in a Fourier series in the angular direction, thus leading to an infinite number of two-dimensional problems. By expressing the boundary conditions in terms of Cartesian components, rather than polar components, the coefficient matrix will be independent of the Fourier order, and the Hankel transforms of all the expansion coefficients for the unknown potentials can be found with only one matrix inversion for each horizontal wavenumber. The truncation point of the Fourier series can be determined *a priori*.

The inversion of the Hankel transform is again performed by means of the fast field technique, and the angular distribution is evaluated from the expansion coefficients by means of an FFT technique. In the following the model and its mathematical background will be described. In order to demonstrate its possibilities, the model has been used to analyze the response of a line array in a simple shallow water environment.

## I. FIELD REPRESENTATIONS

The problem under consideration is illustrated in Fig. 1. A number of simple sources is placed in a horizontally stratified environment. All layers are assumed to be homogeneous and isotropic elastic continua, either fluid or solid. Each source radiates compressional stress waves at the common angular frequency $\omega$. The resulting stresses and displacements can then be expressed in complex form with the common factor $\exp(j\omega t)$. This factor will not be included explicitly in the following sections. Since the sources are assumed to be distributed within a relatively small region compared to the total volume of interest, the field is derived in a cylindrical coordinate system $\{r,\theta,z\}$, Fig. 1.

The field in each layer is a superposition of the field produced by the sources within the layer in the absence of boundaries and an unknown field which is necessary in order to satisfy the boundary conditions at the interfaces. The latter field must satisfy the homogeneous equations of motion and is treated first.

### A. Homogeneous solution

Let $\mathbf{u}_n = \{u_n, v_n, w_n\}$ be the polar displacement components in a solid layer $n$. The homogeneous equation of motion
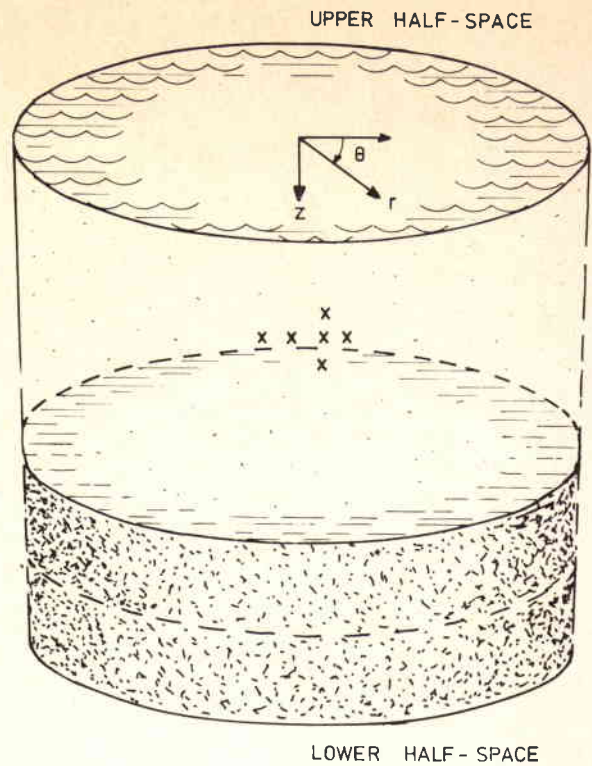


FIG. 1. A general outline of the model geometry.

$$(\lambda_n + 2\mu_n)\nabla\nabla\cdot\mathbf{u}_n - \mu_n\nabla\times\nabla\times\mathbf{u}_n - \rho_n\frac{\partial^2\mathbf{u}_n}{\partial t^2} = 0, \quad (1)$$

where $\lambda_n$ and $\mu_n$ are the Lamé constants and $\rho_n$ is the density, will be satisfied if the displacements are expressed in terms of three scalar potentials $\{\phi_n, \Lambda_n, \psi_n\}$ as[10]

$$u_n = \frac{\partial\phi_n}{\partial r} + \frac{1}{r}\frac{\partial\psi_n}{\partial\theta} + \frac{\partial^2\Lambda_n}{\partial r\partial z}, \quad (2)$$

$$v_n = \frac{1}{r}\frac{\partial\phi_n}{\partial\theta} - \frac{\partial\psi_n}{\partial r} + \frac{1}{r}\frac{\partial^2\Lambda_n}{\partial\theta\partial z}, \quad (3)$$

$$w_n = \frac{\partial\phi_n}{\partial z} - \left(\frac{1}{r}\frac{\partial}{\partial r}r\frac{\partial}{\partial r} + \frac{1}{r^2}\frac{\partial^2}{\partial\theta^2}\right)\Lambda_n, \quad (4)$$

where the potentials satisfy the homogeneous scalar wave equations

$$(\nabla^2 + h_n^2)\phi_n = 0, \quad (5)$$

$$(\nabla^2 + k_n^2)(\Lambda_n, \psi_n) = 0, \quad (6)$$

$h_n$ and $k_n$ are the wavenumbers of compressional and shear waves, respectively,

$$h_n^2 = \omega^2/c_{cn}^2 = \rho_n\omega^2/(\lambda_n + 2\mu_n), \quad (7)$$

$$k_n^2 = \omega^2/c_{sn}^2 = \rho_n\omega^2/\mu_n, \quad (8)$$

where $c_{cn}$ and $c_{sn}$ are the velocities of compressional and shear waves, respectively. The attenuation in the medium can be accounted for by allowing the Lamé constants, and thus, also the wavenumbers, to be complex.

In order to avoid confusion, the index $n$ referring to the layer number will be implied in the rest of this section. The following angular expansions of the potentials are introduced:

$$\phi(r,\theta,z) = \sum_{m=0}^{\infty} \phi^m(r,z) \frac{\cos(m\theta)}{\sin(m\theta)}, \tag{9}$$

$$\Lambda(r,\theta,z) = \sum_{m=0}^{\infty} \Lambda^m(r,z) \frac{\cos(m\theta)}{\sin(m\theta)}, \tag{10}$$

$$\psi(r,\theta,z) = \sum_{m=0}^{\infty} \psi^m(r,z) \frac{\sin(m\theta)}{-\cos(m\theta)}. \tag{11}$$

Substitution of these into the wave equation and use of the Hankel transform lead to the following integral representations for the expansion coefficients:

$$\phi^m(r,z) = \int_0^{\infty} [a_1^m(s)e^{-z\alpha(s)} + a_2^m(s)e^{z\alpha(s)}]sJ_m(rs)\,ds, \tag{12}$$

$$\Lambda^m(r,z) = \int_0^{\infty} [b_1^m(s)e^{-z\beta(s)} + b_2^m(s)e^{z\beta(s)}]J_m(rs)\,ds, \tag{13}$$

$$\psi^m(r,z) = \int_0^{\infty} [c_1^m(s)e^{-z\beta(s)} + c_2^m(s)e^{z\beta(s)}]sJ_m(rs)\,ds, \tag{14}$$

where $J_m(\ )$ is the Bessel function of order $m$ and

$$\alpha(s) = \begin{cases} (s^2 - h^2)^{1/2}, & s^2 > \mathrm{Re}\{h^2\}, \\ j(h^2 - s^2)^{1/2}, & s^2 \leqslant \mathrm{Re}\{h^2\}, \end{cases} \tag{15}$$

$$\beta(s) = \begin{cases} (s^2 - k^2)^{1/2}, & s^2 > \mathrm{Re}\{k^2\}, \\ j(k^2 - s^2)^{1/2}, & s^2 \leqslant \mathrm{Re}\{k^2\}. \end{cases} \tag{16}$$

The displacement components $w$, $u$, and $v$ are expanded like (9), (10), and (11), respectively. If Eqs. (9)–(14) are inserted into Eqs. (2)–(4) the following integral representations are obtained for the expansion coefficients:

$$w^m(r,z) = \int_0^{\infty} [-a_1^m(s)\alpha(s)e^{-z\alpha(s)} + a_2^m(s)\alpha(s)e^{z\alpha(s)} + b_1^m(s)se^{-z\beta(s)} + b_2^m(s)se^{z\beta(s)}]sJ_m(rs)\,ds, \tag{17}$$

$$u^m(r,z) \pm v^m(r,z) = \int_0^{\infty} [\mp a_1^m(s)se^{-z\alpha(s)} \mp a_2^m(s)se^{z\alpha(s)} \pm b_1^m(s)\beta(s)e^{-z\beta(s)}$$
$$\mp b_2^m(s)\beta(s)e^{z\beta(s)} + c_1^m(s)se^{-z\beta(s)} + c_2^m(s)se^{z\beta(s)}]sJ_{m\pm1}(rs)\,ds. \tag{18}$$

The combination of the polar vector components in (18) corresponds to the Cartesian components for Fourier order $m$ and is, therefore, the natural scalar equivalent of the scalar component $w^m$ (see Schmidt and Krenk[10]).

The following boundary conditions at the horizontal interfaces involve the stress components $\sigma_{zz}$, $\sigma_{rz}$, and $\sigma_{\theta z}$. If these are expanded like (9), (10), and (11), respectively, use of Hooke's law leads to the following expressions for the expansion coefficients:

$$\sigma_{zz}^m(r,z) = \lambda \nabla^2 \phi^m(r,z) + 2\mu(\partial/\partial z)w^m(r,z)$$
$$= \mu \int_0^{\infty} [a_1^m(s)(2s^2 - k^2)e^{-z\alpha(s)} + (2s^2 - k^2)a_2^m(s)e^{z\alpha(s)} - b_1^m(s)2s\beta(s)e^{-z\beta(s)} + b_2^m(s)2s\beta(s)e^{z\beta(s)}]sJ_m(rs)\,ds, \tag{19}$$

$$\sigma_{rz}^m(r,z) \pm \sigma_{\theta z}^m(r,z) = \mu \left[ \frac{\partial}{\partial z}[u^m(r,z) \pm v^m(r,z)] + \left( \frac{\partial}{\partial r} \mp \frac{m}{r} \right)w^m(r,z) \right]$$
$$= \mu \int_0^{\infty} [\pm a_1^m(s)2s\alpha(s)e^{-z\alpha(s)} \mp a_2^m(s)2s\alpha(s)e^{z\alpha(s)} \mp b_1^m(s)(2s^2 - k^2)e^{-z\beta(s)}$$
$$\mp b_2^m(s)(2s^2 - k^2)e^{z\beta(s)} - c_1^m(s)s\beta(s)e^{-z\beta(s)} + c_2^m(s)s\beta(s)e^{z\beta(s)}]sJ_{m\pm1}(sr)\,ds. \tag{20}$$

It should be noted that the use of the Cartesian components (18) and (20) in the boundary conditions rather than the polar components has the effect that all coefficients to the unknown arbitrary functions are independent of the Fourier order $m$. This is obviously very important for the efficiency of the numerical solution.

For fluid layers only the potential $\phi(r,\theta,z)$ will be present, and the expansion coefficients for the displacements are obtained directly from (17) and (18) by setting $b_1^m$, $b_2^m$, $c_1^m$, and $c_2^m$ to zero. The shear stresses vanish identically, whereas (19) has to be replaced by

$$\sigma_{zz}^m(r,z) = \lambda \Delta^2 \phi^m(r,z) = -\lambda h^2 \int_0^{\infty} [a_1^m(s)e^{-z\alpha(s)}$$
$$+ a_2^m(s)e^{z\alpha(s)}]sJ_m(rs)\,ds. \tag{21}$$

## B. Source field

A simple compressional source placed at the point $\{r_i, \theta_i, z_i\}$ will produce the following field in an infinite homogeneous medium[11]:

$$\tilde{\phi}_i(r,\theta,z) = \frac{S_i}{4\pi\omega} \sum_{m=0}^{\infty} \epsilon_m \cos(\theta - \theta_i) \int_0^{\infty} \{J_m(r_i s)$$
$$\times [e^{-\alpha(s)|z - z_i|}/\alpha(s)]\}sJ_m(rs)\,ds, \tag{22}$$

where $S_i$ is the source strength, which is generally complex to account for the actual phase of the source. The factor $\epsilon_m$, due to the expansion of the exponential function in a Neumann series,[11] is

$$\epsilon_m = \begin{cases} 1, & m = 0, \\ 2, & m > 0. \end{cases} \tag{23}$$

If more than one source is present within a layer, the contributions are simply added to yield

$$\bar{\phi}(r,\theta,z) = \frac{1}{4\pi\omega} \sum_{m=0}^{\infty} \epsilon_m \int_0^{\infty} \left( \sum_{i=1}^{N} S_i \cos m(\theta - \theta_i) \right.$$

$$\left. \times J_m(r_i s) \frac{e^{-\alpha(s)|z - z_i|}}{\alpha(s)} \right) s J_m(rs) \, ds, \quad (24)$$

where $N$ is the number of sources. The potential $\bar{\phi}(r,\theta,z)$ is now expanded like (9) and the coefficients are easily obtained as

$$\tilde{\phi}^m(r,\theta,z) = \frac{\epsilon_m}{4\pi\omega} \int_0^{\infty} \left( \sum_{i=1}^{N} S_i \frac{\cos(m\theta_i)}{\sin(m\theta_i)} J_m(r_i s) \right.$$

$$\left. \times \frac{e^{-\alpha(s)|z - z_i|}}{\alpha(s)} \right) s J_m(rs) \, ds. \quad (25)$$

The expansion coefficients for the Cartesian displacements components again follow from (2)–(4),

$$\tilde{w}^m(r,\theta,r) = -\frac{\epsilon_m}{4\pi\omega} \int_0^{\infty} \left( \sum_{i=1}^{N} S_i \frac{\cos(m\theta_i)}{\sin(m\theta_i)} \, \mathrm{sgn}(z - z_i) \right.$$

$$\left. \times J_m(r_i s) e^{-\alpha(s)|z - z_i|} \right) s J_m(rs) \, ds, \quad (26)$$

$$\tilde{u}^m(r,z) \pm \tilde{v}^m(r,z) = \mp \frac{\epsilon_m}{4\pi\omega} \int_0^{\infty} \left( s \sum_{i=1}^{N} S_i \frac{\cos(m\theta_i)}{\sin(m\theta_i)} \right.$$

$$\left. \times J_m(sr_i) \frac{e^{-\alpha(s)|z - z_i|}}{\alpha(s)} \right) s J_{m \pm 1}(rs) \, ds, \quad (27)$$

and use of Hooke's law yields the following expansion coefficients for the stresses involved in the boundary conditions

$$\tilde{\sigma}_{zz}^m(r,z) = \frac{\mu \epsilon_m}{4\pi\omega} \int_0^{\infty} \left( (2s^2 - k^2) \sum_{i=1}^{N} S_i \frac{\cos(m\theta_i)}{\sin(m\theta_i)} \right.$$

$$\left. \times J_m(sr_i) \frac{e^{-\alpha(s)|z - z_i|}}{\alpha(s)} \right) s J_m(rs) \, ds, \quad (28)$$

$$\tilde{\sigma}_{rz}^m(r,z) \pm \tilde{\sigma}_{\theta z}^m(r,z)$$

$$= \pm \frac{\mu \epsilon_m}{4\pi\omega} \int_0^{\infty} \left( 2s \sum_{i=1}^{N} S_i \frac{\cos(m\theta_i)}{\sin(m\theta_i)} \right.$$

$$\left. \times \mathrm{sgn}(z - z_i) J_m(sr_i) e^{-\alpha(s)|z - z_i|} \right) s J_{m \pm 1}(sr) \, ds. \quad (29)$$

In the case of a fluid layer, Eq. (28) must be modified to

$$\tilde{\sigma}_{zz}^m(r,z) = -\frac{\lambda h^2 \epsilon_m}{4\pi\omega} \int_0^{\infty} \left( \sum_{i=1}^{N} S_i \frac{\cos(m\theta_i)}{\sin(m\theta_i)} J_m(sr_i) \right.$$

$$\left. \times \frac{e^{-\alpha(s)|z - z_i|}}{\alpha(s)} \right) s J_m(sr) \, ds. \quad (30)$$

Here, only simple compressional sources have been considered, but shear wave sources, involving the potential $\Lambda$ or $\psi$,

can be treated in exactly the same way, leading to integral representations similar to Eqs. (26)–(29) for the field parameters.

## II. SOLUTION TECHNIQUE

Solution of the problem at hand implies finding the values of the potential $a$, $b$, and $c$ that satisfy the pertinent boundary conditions. At each interface $w$ and $\sigma_{zz}$ must be continuous. At solid/solid interfaces we must in addition require that $u$, $v$, $\sigma_{rz}$, and $\sigma_{\theta z}$ be continuous. At solid/liquid interfaces the shear stresses must vanish.

We express these boundary conditions with (2), (3), and (4) and the expressions for stresses obtained by the use of Hookes law. These boundary conditions may readily be reformulated in terms of the angular expansion coefficients which, when collected in a column vector, become

$$F^m(r,z) = \begin{pmatrix} w^m(r,z) \\ u^m(r,z) + v^m(r,z) \\ u^m(r,z) - v^m(r,z) \\ \sigma_{zz}^m(r,z) \\ \sigma_{rz}^m(r,z) + \sigma_{\theta z}^m(r,z) \\ \sigma_{rz}^m(r,z) - \sigma_{\theta z}^m(r,z) \end{pmatrix}. \quad (31)$$

The unknown potentials are so defined that the depth coordinate $z$ within this layer is 0 at the upper layer interface. The boundary conditions at interface $n$, which is the lower interface of layer $n$, may thus be stated:

$$F_n^m(r,z_n) + \tilde{F}_n^m(r,z_n) - F_{n+1}^m(r,0) - \tilde{F}_{n+1}^m(r,0) = 0, \quad (32)$$

where subscript $n$ denotes the layer number, $z_n$ denotes the thickness of layer $n$, and the terms with overbar "~", as before, denote source terms.

Insertion of (17), (18), (19) [(21) in the fluid case], and (20), reduces (32) to a set of integrands which must vanish as the boundary conditions must be satisfied for all $r$. Thus we are left with a set of linear equations in the unknown potential functions and the source contributions:

$$A_{n,l} B_n^m - A_{n+1,u} B_{n+1}^m = R_{n+1,u}^m - R_{n,l}^m, \quad (33)$$

where the unknown potential functions for layer $n$ are

$$B_n^m(s) = \begin{pmatrix} a_{1,n}^m(s) \\ b_{1,n}^m(s) \\ c_{1,n}^m(s) \\ a_{2,n}^m(s) \\ b_{2,n}^m(s) \\ c_{2,n}^m(s) \end{pmatrix}. \quad (34)$$

For a solid layer the matrix $A$ for the upper interface in layer $n$ is

$$A_{n,u}(S) = \begin{pmatrix} -\alpha & s & 0 & \alpha & s & 0 \\ -s & \beta & s & -s & -\beta & s \\ s & -\beta & s & s & \beta & s \\ (2s^2 - k^2)\mu & -2s\beta\mu & 0 & (2s^2 - k^2)\mu & 2s\beta\mu & 0 \\ 2s\alpha\mu & -(2s^2 - k^2)\mu & -s\beta\mu & -2s\alpha\mu & -(2s^2 - k^2)\mu & s\beta\mu \\ -2s\alpha\mu & (2s^2 - k^2)\mu & -s\beta\mu & 2s\alpha\mu & -(2s^2 - k^2)\mu & s\beta\mu \end{pmatrix}, \quad (35)$$

H. Schmidt and J. Glattetre: Global matrix method for waves

while for a liquid layer, the matrix becomes

$$A_{n,u}(S) = \begin{pmatrix} -\alpha & 0 & 0 & \alpha & 0 & 0 \\ -s & 0 & 0 & -s & 0 & 0 \\ s & 0 & 0 & s & 0 & 0 \\ -\lambda h^2 & 0 & 0 & -\lambda h^2 & 0 & 0 \\ 0 & 0 & 0 & 0 & 0 & 0 \\ 0 & 0 & 0 & 0 & 0 & 0 \end{pmatrix}. \tag{36}$$

The matrix for the lower interface of a layer is obtained by multiplying each element with the appropriate exponential as given by (17)–(21) with $z = z_n$, i.e.,

$$A_{n,1}(S) = A_n(S)I_n(S), \tag{37}$$

where

$$I_n(S) = \begin{pmatrix} e^{-\alpha(s)z_n} & 0 & 0 & 0 & 0 & 0 \\ 0 & e^{-\beta(s)z_n} & 0 & 0 & 0 & 0 \\ 0 & 0 & e^{-\alpha(s)z_n} & 0 & 0 & 0 \\ 0 & 0 & 0 & e^{\alpha(s)z_n} & 0 & 0 \\ 0 & 0 & 0 & 0 & e^{\beta(s)z_n} & 0 \\ 0 & 0 & 0 & 0 & 0 & e^{\beta(s)z_n} \end{pmatrix}. \tag{38}$$

The source contribution vector is

$$R_n^m = \frac{\epsilon_m}{4\pi\omega} \sum_{i=1}^{N} S_i \begin{array}{c} \cos(m\theta_i) \\ \sin(m\theta_i) \end{array} J_m(sr_i)e^{-\alpha|z-z_i|} \begin{pmatrix} -\text{sgn}(z-z_i) \\ -s/\alpha \\ s/\alpha \\ \mu(2s^2 - k^2)/\alpha \\ 2s\mu\,\text{sgn}(z-z_i) \\ -2s\mu\,\text{sgn}(z-z_i) \end{pmatrix}, \tag{39}$$

where of course $z = 0$ and $z_n$ for upper and lower boundaries, respectively. Finally, the local sets of boundary equations for $N$ layers are mapped into a global set of equations

$$\begin{pmatrix} [A_{1,l}] & [-A_{2,u}] & & & \\ & [A_{2,l}] & [-A_{3,u}] & & \\ & & [A_{3,l}] & [-A_{4,u}] & \\ & & & \bullet & \bullet \\ & & & \bullet & \\ & & & [A_{N-1,l}] & [-A_{N,u}] \end{pmatrix} \begin{pmatrix} B_1^m \\ B_2^m \\ \vdots \\ B_N^m \end{pmatrix} = \begin{pmatrix} R_{2,u}^m \\ R_{3,u}^m \\ R_{4,u}^m \\ \vdots \\ R_{N,u}^m \end{pmatrix} - \begin{pmatrix} R_{1,l}^m \\ R_{2,l}^m \\ R_{3,l}^m \\ \vdots \\ R_{N-1,l}^m \end{pmatrix}. \tag{40}$$

This global matrix method, as opposed to matrizant methods,[5] was presented for the two-dimensional case in Ref. 9.

## III. NUMERICAL STABILITY CONSIDERATIONS

A commonly known problem with the matrizant method, on which earlier FFP models have been based,[3] is encountered when dealing with thick layers in the evanescent region of the horizontal wavenumber spectrum. In this region the growing and decaying potentials can differ significantly in magnitude, and the exponential matrix (38) becomes numerically singular when the difference exceeds the number of available digits. In propagator approaches this problem requires considerable, purely numerical, modifications in order to ensure numerical stability at the cost of a significant increase in calculation time. In the present global approach, however, unconditional stability can be ensured by simple means with no influence on the computation time. A detailed analysis is given in Ref 9; only an outline shall be given here. Several techniques are utilized to remedy this situation.

The matrices $A_{n,l}$ and $A_{n,u}$ are made dimensionless by dividing the stress- and displacement-related coefficients by $\omega^2\rho_m$ and $k_m$, respectively. Here, $\rho_m$ and $k_m$ denote the density and wavenumber, respectively, of an intermediate layer. This will ensure that the coefficients are within the same order of magnitude. Each layer is described in a separate local coordinate system with origin at its upper surface. This will ensure that the value of the depth does not exceed the layer thickness. The order of the unknown functions as defined by (34) ensures that the coefficients, which attain high values due to the abovementioned exponential functions, come close to the diagonal of the global matrix. These remedies will, together with standard pivoting by columns, ensure that the solution of (40) by means of Gaussian elimination will be unconditionally stable.[9]

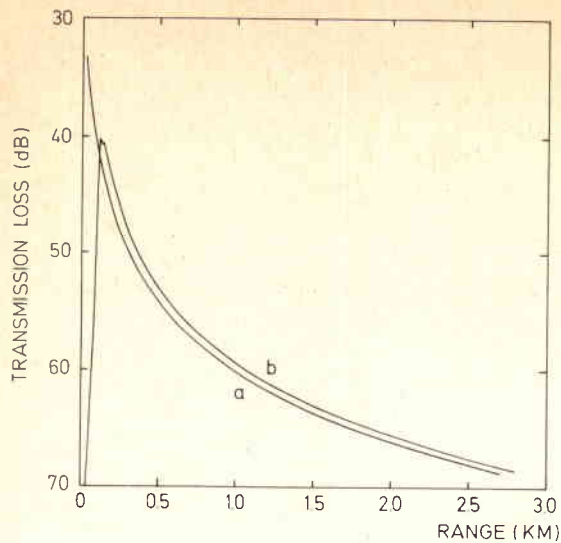The above statement must, however, be slightly modified when we have a source in a thick layer with evanescent

FIG. 2. Transmission loss for a free-space environment. The receiver is located 40 m above the source: (a) source at center axis ($r = 0$), i.e., two-dimensional case; (b) source displaced 100 m in positive $x$ direction, i.e., three-dimensional case.

propagation conditions. Here, numerical instability due to the nonvanishing pertinent row of the right-hand side of (40) may occur. This problem is easily circumvented by introducing dummy interfaces just above and below the source(s). Coherent sources on both sides of a thick layer may also represent a numerical problem, but as this situation is regarded as being less important in most physical applications, it is not considered a serious limitation. It is of course possible to solve the problem separately for both these sources and superpose the solutions.

## IV. NUMERICAL EXAMPLES

### A. A point source in free-space

The example of a point source in free-space is a well-suited example for verification of the model as the correct result is readily calculated as 20 log($r$). "Free-space" means a water layer containing source and receiver, surrounded by upper and lower half-spaces consisting of water with identical parameters. This example is, however, rather a challenge for the FFP model, as the integrand easily becomes undersampled due to the branch point arising from the square root in the denominator of (28). Here, the integrand is sampled at 8196 points ranging from $628 \times 10^{-6}$ m$^{-1}$ to 0.465 m$^{-1}$.

Figure 2 shows a comparison between model outputs with the source located on the center axis and also with the source displaced 100 m in the positive $x$ direction from the center axis, i.e., the model is run in two- and three-dimensional modes, respectively. In both cases the frequency is 100 Hz and the receiver is located 40 m above the source. The three-dimensional case required an angular expansion order of 110. Curves a and b show the transmission loss for the two-dimensional and three-dimensional cases, respectively. The region of validity for the computed solution begins at a greater distance from the source in the three-dimensional case, as the approximation to the higher-order Hankel functions has larger remainders than what is the case for the zero-order approximation. The computed solution is of course not valid between the source and center axis as only the Hankel function corresponding to outward propagating waves is included. Figure 3 shows the computed transmission loss in all directions for the three-dimensional example. The line markers $x \equiv 0$ and $y \equiv 0$ are drawn.
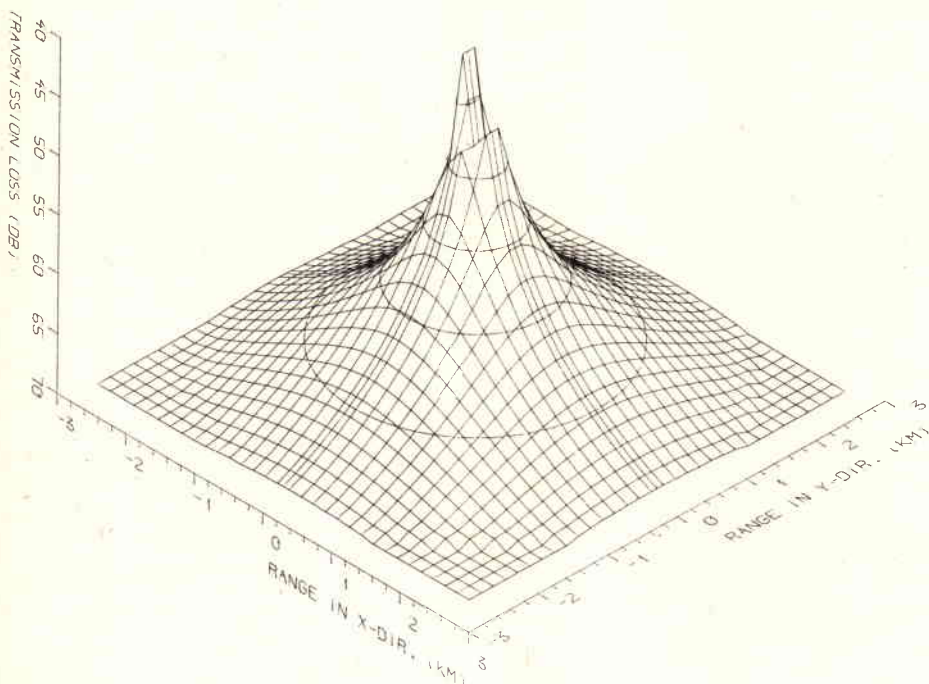


FIG. 3. Polar plot of transmission loss for a point source in free-space, the source displaced 100 m in the positive $x$ direction.

```
                    VACUUM
  0 m  ─────────────────────────────────
                    WATER

        ρ = 1 g/cm³
        P-wave: vel.: 1480 m/s  att.: ≈0
        S-wave: vel:   0
 75 m  ─────────────────────────────────
              SHALE - SANDSTONE

        ρ = 2.55 g/cm³
        P-wave: vel.: 4500 m/s  att.: 0.5 dB/λ
        S-wave: vel.: 2250 m/s  att.: 1.9 dB/λ
975 m  ─────────────────────────────────
              SHALE - SANDSTONE

        ρ = 2.7 g/cm³
        P-wave: vel.: 5300 m/s  att.: 0.3 dB/λ
        S-wave: vel.: 2650 m/s  att.: 1.1 dB/λ
1975 m ─────────────────────────────────

        ρ = 2.8 g/cm³
        P-wave: vel.: 5800 m/s
        S-wave: vel.: 2800 m/s
```
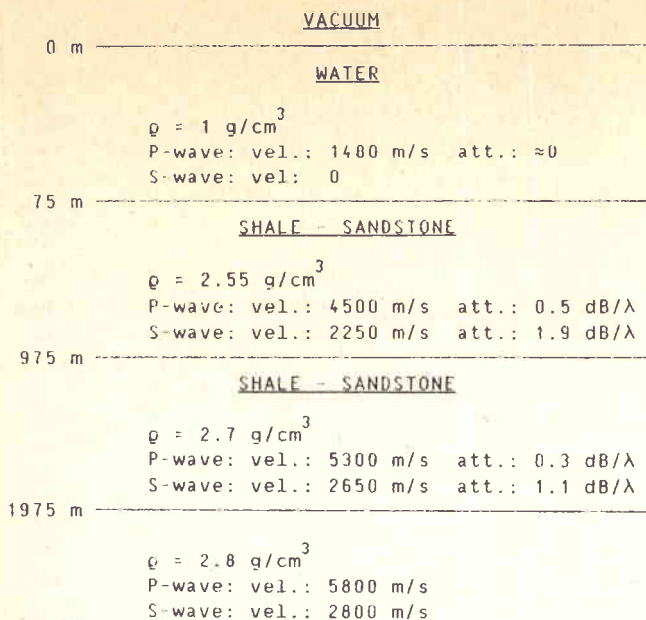
FIG. 4. The environmental conditions of the test case.

## B. Shallow water propagation

We will further demonstrate some of the model's capabilities by applying it to some propagation problems related to the shallow water environment shown in Fig. 4.

Below a 75-m-deep homogeneous water layer are three solid layers with increasing density and wave velocities. Our study will concentrate on the water layer and on one occasion take us 125 m below the ocean-bottom interface. The compressional wave acoustic impedance ratio at the ocean-bottom interface is approximately 7.8, thus giving strong bottom reflections.

### 1. Point source

We will first look into the basic wave propagation mechanisms by studying the frequency versus horizontal wavenumber response of a point source, at 10-m water depth, up to a frequency of 50 Hz. Figure 5 shows the dispersion relation for the pressure component at 70-m water depth. The vertical axis is linear with an arbitrary scale. The curves in Fig. 5 are actually the modulus of the integrand entering the FFT approximation to the Hankel transform.

The six line markers radiating from the origin show the loci of the critical horizontal wavenumbers for compressional and shear waves at the boundaries. They are, as appearing in increasing horizontal wavenumber order: compressional critical wavenumber for boundaries at 1975, 975, and 75 m; shear critical wavenumber for the boundaries at 1975, 975, 75 m. The spikes, associated with the compressional critical wavenumbers, represent head waves. Above the shear critical wavenumber for the 75-m-deep water-bottom interface, we can, as expected, observe that the group velocity of the modes approaches the phase velocity asymptotically.

Figure 6 shows the same integrand as Fig. 5 in a depth versus horizontal wavenumber plot for a frequency of 35 Hz.
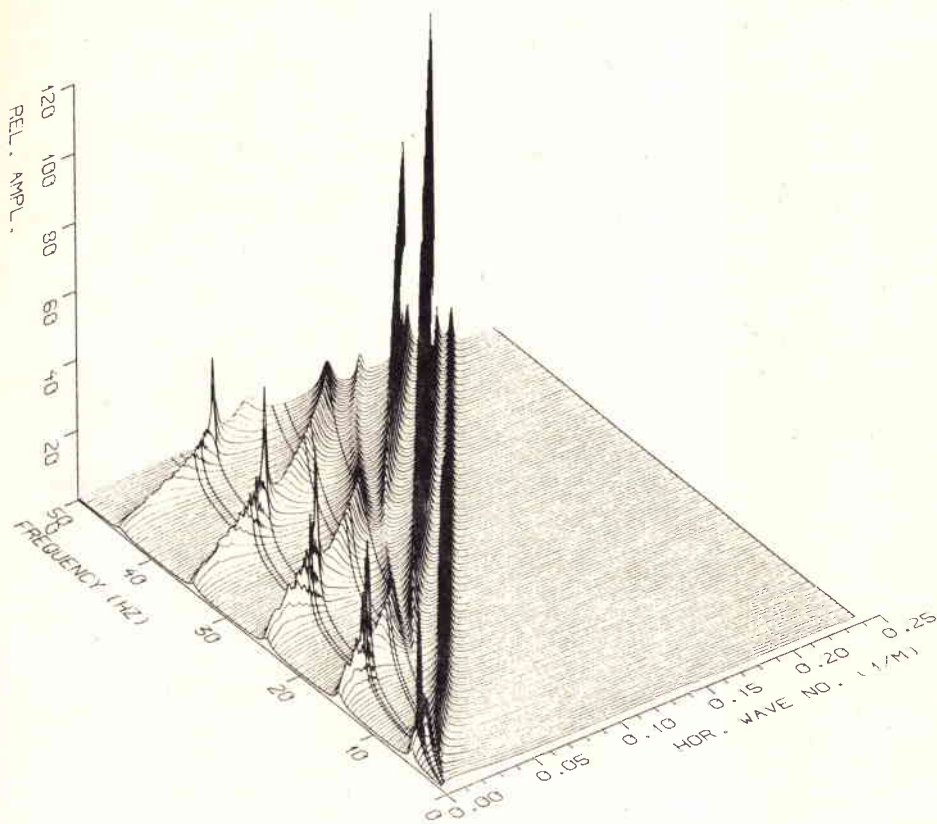


FIG. 5. Modulus of pressure integrand shown as frequency versus horizontal wavenumber. Line markers are, as appearing in increasing horizontal wavenumber order: compressional critical wavenumber for boundaries at 1975, 975, and 75 m; shear critical wavenumber for the boundaries at 1975, 975, and 75 m.
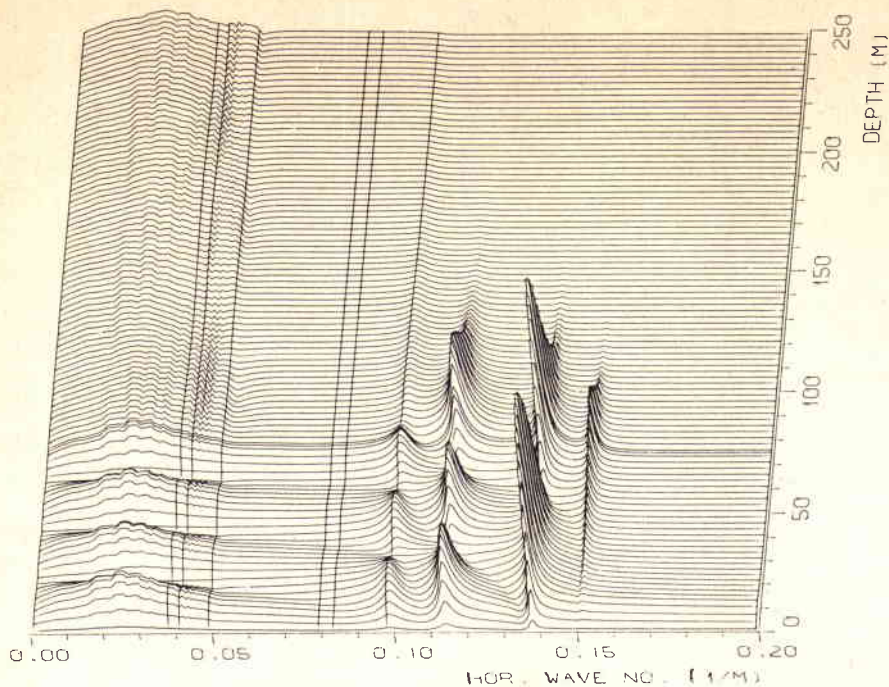
FIG. 6. Modulus of pressure integrand shown as depth versus horizontal wavenumber. Line markers are, as appearing in increasing horizontal wavenumber order: compressional critical wavenumber for boundaries at 1975, 975, and 75 m; shear critical wavenumber for the boundaries at 1975, 975, and 75 m and water-ocean boundary at 75 m.

For depths larger than 75 m, i.e., down into the bottom, the actual parameter is stress $\sigma_{zz}$. In a solid, it represents the compressional wave component modified by shear components. Line markers indicate the same horizontal wavenumbers as in Fig. 5 and also the water-bottom boundary at 75 m.

As phase velocities increase with depth, it is apparent that the effective depth of the propagation channel will increase with decreasing horizontal wavenumber. Furthermore, as losses are introduced in the solid layers, the propagation channel will show greater dissipative losses at lower wavenumbers. Below the critical horizontal wavenumber for shear waves at the basement interface, 0.079 m$^{-1}$, energy leaks out into the basement and we do not have a well-defined propagation channel. Thus, starting from the upper wavenumber end of Fig. 6, the first two modes propagate in the water layer and, consequently, have low losses. The third mode also propagates in the water layer, but dissipation occurs due to evanescent energy injection into the ocean bottom. From the fourth mode and below, we observe transition to a continuous spectrum, where the losses are caused by both dissipation and energy outflow.

### 2. Linear array

In order to exploit the three-dimensional capability of the model, we introduce a linear array consisting of 101 elements equispaced at 18.6 m. The array is aligned with the axes $\theta = 0$, $z = 45$ m and centered about the axis $r = 0$. The elements are excited so as to produce a "narrow" horizontal wavenumber spectrum in the direction $\theta = 0$ corresponding to mainlobes at $\theta = \pm 60$ in the horizontal plane when the array is in an all-water environment.

Figure 7 shows a polar plot of the pressure level in a horizontal plane at 47-m water depth. It can be seen that energy is propagating in several distinct directions at azi-

muthal angles in the order of 60° and less. One could initially assume these directions to be sidelobes of the array. There are, however, three points that contradict this assumption: The azimuthal dependence is not in accordance with what should be expected from a 101-element array, attenuation versus range is significantly different in various azimuthal directions, and one does not see a range-dependent interference pattern as would normally be caused by multimode interference.

Further insight is gained by depicting the pressure level versus depth and azimuthal angle as in Fig. 8, where we are able to identify the mode structure which was illustrated in Fig. 6. The propagating energy concentrated at azimuthal angles in the order of $\pm 60°$ and less is clearly split up into slightly different directions, each being characterized by a unique mode and thus a unique horizontal wavenumber. The first-order mode is visible when observing the positive azimuthal angle part of Fig. 8. The characteristic contours of the higher-order modes become visible "on the far side of the mountain," i.e., when observing the negative azimuthal angle part of the figure.

The physical explanation for the mode separation is that the array will produce a continuous horizontal wavenumber spectrum ranging from $\omega/c$ at $\theta = \pm 60°$ to $\omega/2c$ at $\theta = 0°$. However, as we remember from Fig. 6, our stratified medium will support energy transmission at discrete components of horizontal wavenumber. Thus, as we see from Fig. 8, energy is transmitted at the angles where the horizontal wavenumber of the array is matched to the discrete values of horizontal wavenumber corresponding to the discrete modes.

In returning to Fig. 7, we see that the four single mode beams are pointing towards us, while for the other side of the array, i.e., in the positive $x$ and $y$ direction, we can see the second-, third-, and fourth-order modes. It is clear that the

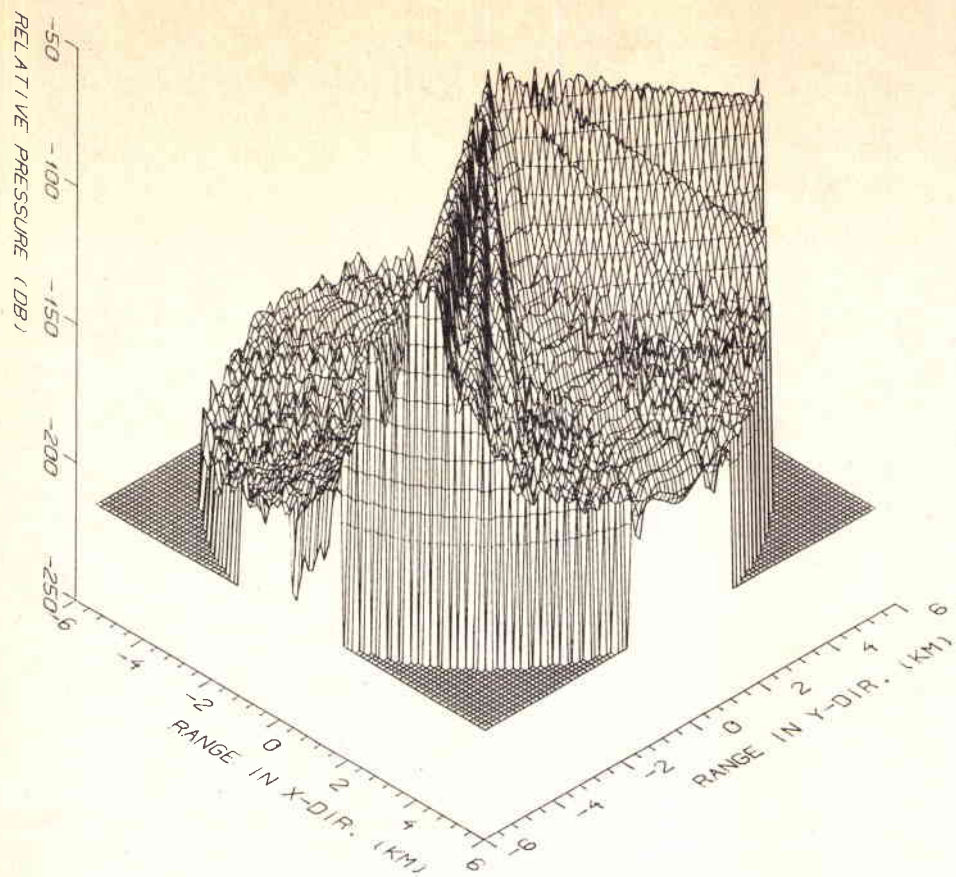H. Schmidt and J. Glattetre: Global matrix method for waves

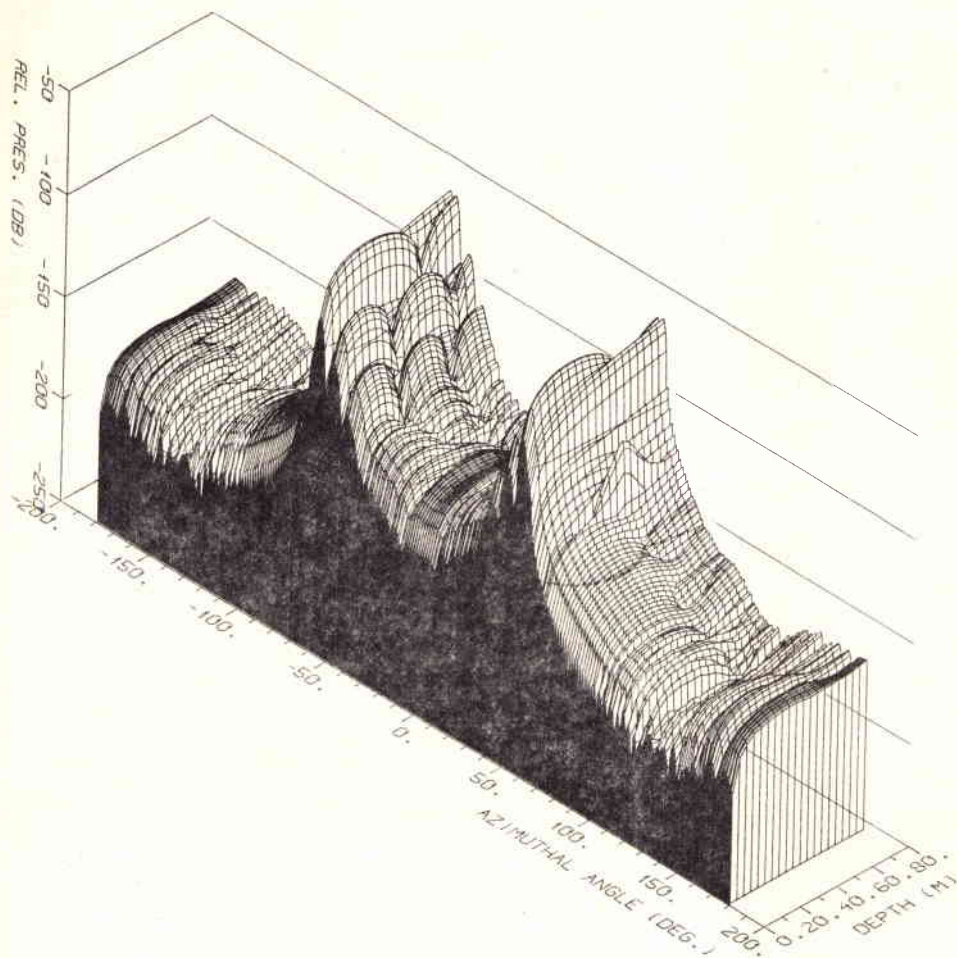FIG. 7. Polar plot of pressure at 47-m water depth. Isolines spaced 10 dB.



FIG. 8. Pressure at 2.8-km range shown as azimuthal angle versus depth.

third- and fourth-order modes suffer greater transmission loss as discussed above.

## V. CONCLUSIONS

A three-dimensional FFP model based on the global matrix method has been presented. The global matrix method allows for a more efficient and, furthermore, numerically stable computation. The three-dimensional expansion does not restrict sources to be on the center axis, but allows for an arbitrary source geometry, as opposed to earlier two-dimensional versions. As a consequence, the solution includes both vertically and horizontally polarized shear waves simultaneously. A mathematical description is given and the numerical aspects are discussed. Some of the model's capabilities are illustrated in two test cases: free-space and shallow water with a strongly reflecting bottom. The free-space case shows that the three-dimensional solution gives results identical to those obtained by the two-dimensional solution except for ranges close to the axis $r \equiv 0$ of a cylindrical coordinate system. For the shallow water case, it has been demonstrated that energy is transported in discrete modes above the critical wavenumbers, and that, when excited by a long linear array, different modes will propagate in slightly different directions.

## ACKNOWLEDGMENTS

[1]W. M. Ewing, W. S. Jardetzky, and F. Press, *Elastic Waves in Layered Media* (McGraw-Hill, New York, 1957).

[2]H. W. Marsh, M. Shulkin, and S. G. Kneale, "Scattering of Underwater Sound by the Sea Surface," J. Acoust. Soc. Am. **33**, 334–340 (1961).

[3]F. R. DiNapoli and R. L. Deavenport, "Theoretical and Numerical Green's Function Solution in a Plane Multilayered Medium," J. Acoust. Soc. Am. **67**, 92–105 (1980).

[4]W. T. Thomson, "Transmission of Elastic Waves Through a Stratified Solid Medium," J. Appl. Phys. **21**, 89–93 (1950).

[5]N. A. Haskell, "The Dispersion of Surface Waves on Multilayered Media," Bull. Seismol. Soc. Am. **43**, 17–34 (1953).

[6]F. R. DiNapoli, "Fast Field Program for Multilayered Media," Rep. 4103, U.S. Naval Underwater Systems Center, New London, CT (1971).

[7]H. W. Kutschale, "Rapid Computation by Wave Theory of Propagation Loss in the Artic Ocean," Rep. CU-8-73, Columbia University, Palisades, NY (1973).

[8]C. H. Harrison, "Modelling Low Frequency Sound Propagation in Solid/ Fluid Layers," in *Acoustics and the Sea-Bed* (Bath U.P., Bath, England, 1983), pp. 233–239.

[9]H. Schmidt and F. B. Jensen, "A Full Wave Solution for Propagation in Multilayered Viscoelastic Media with Application to Gaussian Beam Reflection at Fluid–Solid Interfaces," J. Acoust. Soc. Am. **77**, 813–825 (1985).

[10]H. Schmidt and S. Krenk, "Asymmetric Vibrations of a Circular Elastic Plate on an Elastic Half-Space," Int. J. Solids Struct. **18**, 91–105 (1982).

[11]P. M. Morse and K. U. Ingard, *Theoretical Acoustics* (McGraw-Hill, New York, 1968).

KEYWORDS

BOTTOM REFLECTION
FAST FIELD MODEL
FAST FIELD PROGRAM
FFP
FREE-SPACE
GLOBAL MATRIX METHOD
HANKEL TRANSFORM
LONG LINEAR ARRAY
SHALLOW WATER
SHEAR WAVES
STRATIFIED ENVIRONMENTS
THREE-DIMENSIONAL WAVE PROPAGATION

## INITIAL DISTRIBUTION

Copies                                Copies

### MINISTRIES OF DEFENCE

| | |
|---|---|
| JSPHQ Belgium | 2 |
| DND Canada | 10 |
| CHOD Denmark | 8 |
| MOD France | 8 |
| MOD Germany | 15 |
| MOD Greece | 11 |
| MOD Italy | 10 |
| MOD Netherlands | 12 |
| CHOD Norway | 10 |
| MOD Portugal | 2 |
| MOD Spain | 2 |
| MOD Turkey | 5 |
| MOD U.K. | 20 |
| SECDEF U.S. | 68 |

### NATO AUTHORITIES

| | |
|---|---|
| Defence Planning Committee | 3 |
| NAMILCOM | 2 |
| SACLANT | 10 |
| SACLANTREPEUR | 1 |
| CINCWESTLANT/COMOCEANLANT | 1 |
| COMSTRIKFLTANT | 1 |
| COMIBERLANT | 1 |
| CINCEASTLANT | 1 |
| COMSUBACLANT | 1 |
| COMMAIREASTLANT | 1 |
| SACEUR | 2 |
| CINCNORTH | 1 |
| CINCSOUTH | 1 |
| COMNAVSOUTH | 1 |
| COMSTRIKFORSOUTH | 1 |
| COMEDCENT | 1 |
| COMMARAIRMED | 1 |
| CINCHAN | 3 |

### SCNR FOR SACLANTCEN

| | |
|---|---|
| SCNR Belgium | 1 |
| SCNR Canada | 1 |
| SCNR Denmark | 1 |
| SCNR Germany | 1 |
| SCNR Greece | 1 |
| SCNR Italy | 1 |
| SCNR Netherlands | 1 |
| SCNR Norway | 1 |
| SCNR Portugal | 1 |
| SCNR Turkey | 1 |
| SCNR U.K. | 1 |
| SCNR U.S. | 2 |
| SECGEN Rep. SCNR | 1 |
| NAMILCOM Rep. SCNR | 1 |

### NATIONAL LIAISON OFFICERS

| | |
|---|---|
| NLO Canada | 1 |
| NLO Denmark | 1 |
| NLO Germany | 1 |
| NLO Italy | 1 |
| NLO U.K. | 1 |
| NLO U.S. | 1 |

### NLR TO SACLANT

| | |
|---|---|
| NLR Belgium | 1 |
| NLR Canada | 1 |
| NLR Denmark | 1 |
| NLR Germany | 1 |
| NLR Greece | 1 |
| NLR Italy | 1 |
| NLR Netherlands | 1 |
| NLR Norway | 1 |
| NLR Portugal | 1 |
| NLR Turkey | 1 |
| NLR UK | 1 |
| NLR US | 1 |

| | |
|---|---|
| Total initial distribution | 249 |
| SACLANTCEN Library | 10 |
| Stock | 21 |
| Total number of copies | 280 |